Vertically Oriented Propylene Carbonate Molecules and Tetraethyl Ammonium Ions in Carbon Slit Pores

Masafumi Fukano,[†] Toshihiko Fujimori,[‡] Julie Ségalini,[§,∥] Etsuro Iwama,[§,∥] Pierre-Louis Taberna,[§,∥] Taku Iiyama,[⊥] Tomonori Ohba,[†] Hirofumi Kanoh,[†] Yury Gogotsi,[¶] Patrice Simon,[§,∥] and Katsumi Kaneko*[,‡]

[†]Graduate School of Science, Chiba University, 1-33 Yayoi-cho, Inage-ku, Chiba 263-8522, Japan

[‡]Research Center for Exotic Nanocarbons (JST), Shinshu University, 4-17-1 Wakasato, Nagano City 380-8553, Japan

[§]Centre Inter-universitaire de Recherche et d'Ingénierie des Matériaux, UMR CNRS 5085, Paul Sabatier University, 31062 Toulouse Cedex 4, France

[∥]Réseau National sur le Stockage Electrochimique de l'Energie (RS2E), FR CNRS 3459, France

[⊥]Faculty of Science, Shinshu University, 3-1-1 Asahi, Matsumoto, Nagano 390-8621, Japan

[¶]Department of Materials Science and Engineering, Drexel University, 3141 Chestnut Street, Philadelphia, Pennsylvania 19104, United States

ABSTRACT: We report the vertical alignment of propylene carbonate (PC) molecules interacting with Et_4N^+ and BF_4^- which are confined in extremely narrow slit pores ($w \sim 0.7$ nm) of carbide-derived carbon and pitch-based activated carbon fiber. On the basis of X-ray diffraction (XRD), electron radial distribution function analysis reveals that the nearest PC−PC distance is 0.05−0.06 nm shorter than that in the bulk solution, indicating dense packing of PC molecules in the pores. This confinement effect results from the vertically aligned PC molecules, which are indicated by the reverse Monte Carlo analysis. The ensemble structure of PC molecules in the subnanometer carbon pores will provide better understanding the supercapacitor function.

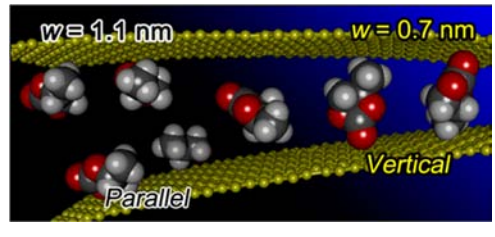

INTRODUCTION

The global trend directed toward the decreasing the use of fossil fuels and nuclear energy has made the issue of safe storage of electric energy even more important than ever. There are nowadays two solutions for electrochemical energy storage: Batteries and supercapacitors that are complementary regarding their power/energy performance. In the case of supercapacitors, a marked increase in the capacitance has been achieved in the past few years.[1−5] Supercapacitor electrodes contain ions in the micropores of carbon, with the size slightly larger than the ion size. Therefore, "the ionic solution" in narrow carbon spaces should be different from the bulk solution. It has been recently shown that molecules and ions in carbon micropores may acquire different structures depending on the pore size. For instance, nanoscale crystalline structures can form in carbon micropores even above the melting temperature of the bulk solid.[6,7] More recently, the high-pressure phase of KI, which needs 1.9 GPa for transformation from the ambient pressure phase, was observed in cylindrical single-walled carbon pores below 0.1 MPa.[8] Extended X-ray absorption fine structure (EXAFS) analysis evidenced the presence of partially dehydrated alkali metal ions in the carbon micropores.[9] Thus, confinement of ions and molecules in nanoscale pores may induce their unusual arrangement. In case of the confinement of neutral molecules, the attractive interaction originates from the dispersion interaction, and the interaction extent is limited in 1−2 nm for a small molecule such as N_2. On the contrary, electrostatic interaction is a longer range interaction, and the ion in the micropore can influence another ion at a larger distance than the size of the ion and the solvent molecules. Accordingly, the ionic solution structure in the carbon micropores can differ from the bulk ionic solution. Theoretical studies also have shown the necessity of improved understanding of highly concentrated ions in the carbon pores.[10−13] In our previous work, X-ray scattering was used for elucidating the structure of organic electrolytic solution constrained in carbon pores of 1.0 nm in the average pore width; the addition of bulky electrolytic ions in the organic solvent in the carbon pore spaces brought about a marked change in the solvent distribution.[14] Chmiola et al.[15] showed that even bulky organic cations could be accommodated in subnanometer scale carbon pores—less than 1 nm in width—using carbide-derived carbons (CDCs). Moreover, a slight decrease of the pore width only by 0.4 nm induced a more than 2-fold increase in the capacitance.

dx.doi.org/10.1021/jp311896q

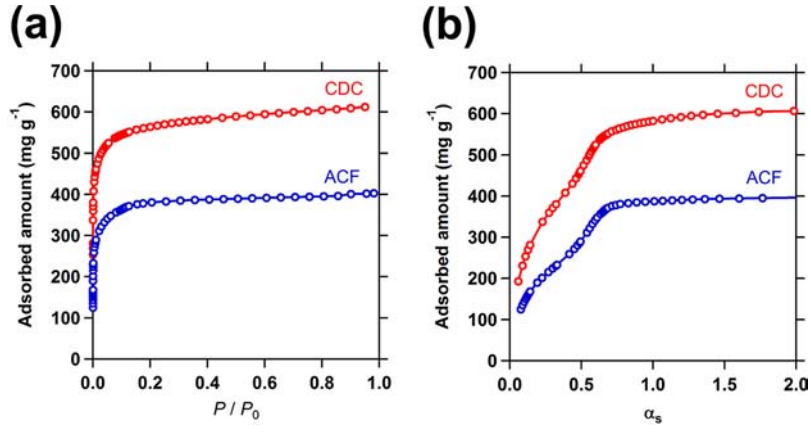

Figure 1. N_2 adsorption isotherms of CDC and ACF at 77 K (a) and their high-resolution α_s plots (b).

This indicates distinctly that the structure of confined organic molecules/ions is highly sensitive to the pore width in the subnanometer range. Consequently, there is a need to elucidate the structure of organic electrolyte in the subnanometer carbon pores to understand the molecular packing as the first step toward understanding the supercapacitor operation. In this paper, the distribution of Et_4NBF_4 and propylene carbonate (PC) molecules in porous carbons with pores of ~0.7 nm is discussed. Here we used samples of CDC and pitch-based activated carbon fiber (ACF).

EXPERIMENTAL METHODS

CDC and ACF were used after grinding in an agate mortar. The N_2 adsorption isotherms of CDC and ACF were measured at 77 K volumetrically using automatic adsorption equipment after the preheating at 393 K and 1 mPa for 2 h. The surface area and microporosity of these carbon samples were determined from the N_2 adsorption isotherms.

X-ray photoelectron spectroscopy (XPS) spectra were measured using a monochromatized Al Kα X-ray source under 10^{-6} Pa (AXIS-ULTRA DLD, Shimazu).

Nanoporous carbon sample was pretreated at 393 K and 1 mPa for 2 h, and then it was immersed in PC and 0.5 M Et_4NBF_4–PC solution. The PC and Et_4NBF_4 deposited on the external surface of the nanoporous carbon were evaporated at 373 K for 3 h under a N_2 flow of 100 mL min^{-1}. The residual amount of PC and/or Et_4NBF_4 on the external surface was less than 10%, which was determined by thermal gravimetric (TG) analysis (Supporting Information, Figure S1).

The synchrotron X-ray diffraction (XRD) patterns of the solution-impregnated carbons and dry carbon samples were measured at 303 K by use of beamline BL02B2, SPring-8, where the wavelength of the incident X-ray was 0.1002 nm. Also the synchrotron XRD patterns of bulk PC and Et_4NBF_4–PC solution were measured for comparison; the Lindemann glass capillary cell of 0.5 mm in diameter was used. The PC or Et_4NBF_4–PC solution embedded carbon was regarded as a three-phase mixed system consisting of molecules and/or ions in the pores, solid carbon, and vacant pore spaces. The necessary X-ray scattering from the interference term between adsorbed molecules in the pore was extracted according to the procedures given in the preceding papers.[6,14]

The reverse Monte Carlo (RMC) simulation was carried out using the XRD data on the interference term between molecules in the carbon pores after the correction procedures. The probable molecular arrangement was deduced, which agreed with experimental XRD data after the above correction. Recent simulation studies have encouraged the use of a more realistic pore model.[16−18] However, a slit-shaped carbon model consisting of double graphene sheets was used for the RMC simulation, because the three-phase mixed system in the nonslit-shaped pore is too complex for simulation and the breadth of the graphitic wall units from XRD is about 3 nm (3.0 nm for CDC and 3.4 nm for ACF), indicating the interaction of molecules with the flat graphitic walls. As to PC and Et_4NBF_4, we used a fully atomistic model. We did not take into account contribution of surface oxygen atoms in the RMC procedure. A new configuration was generated in an RMC trial that was randomly chosen by moving (including rotation), inserting, and deleting a molecule. The ratio of the number of molecules of Et_4NBF_4 and PC was fixed in the calculation, being determined from the experimental conditions. The RMC simulation was repeated over 5 000 000 steps until there was no more improvement in the fitting between simulated XRD pattern and the experimental one. In this RMC, the atomic configuration of molecules in the pore was optimized and no molecular structural distortion was assumed.

RESULTS AND DISCUSSION

Figure 1 shows N_2 adsorption isotherms of as-received CDC and ACF at 77 K and their α_s plots. Both isotherms are of IUPAC type I, indicating that both carbons are microporous. Correspondingly, the high-resolution α_s plots have a clear upward swing below $\alpha_s = 0.5$, indicating that both carbons have very narrow distributions of micropores of less than 1 nm in width.[19] We can determine precisely the specific surface area and micropore volume of both carbons using the subtracting pore effect (SPE) method,[20] as listed in Table 1. The SPE surface area of CDC is much larger than that of ACF, and thereby CDC should have thinner pore walls than ACF. The average slit pore widths of CDC and ACF are almost similar regardless of the great difference in the SPE surface area. The N_2 adsorption analysis evidences that both carbons are almost ultramicroporous. The chemistry of pore walls of CDC and ACF was examined by XPS (see the Supporting Information).

Table 1. Parameters of Pore Structures of CDC and ACF

carbon	S_{α_s}/m^2 g^{-1}	V_{α_s}/cm^3 g^{-1}	w/nm
CDC	1640	0.59	0.72
ACF	1160	0.47	0.75

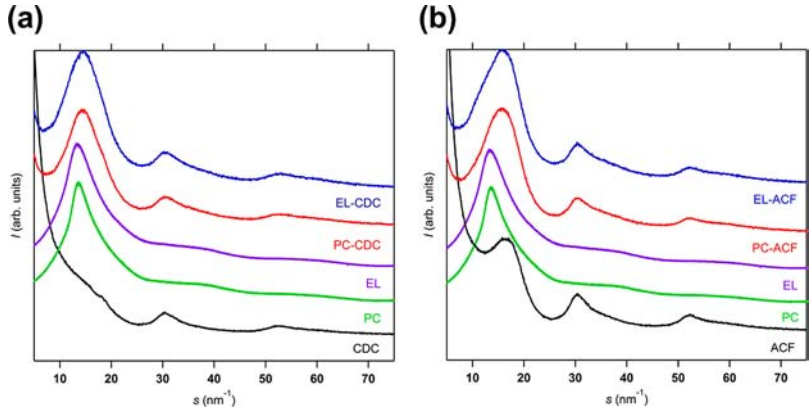

Figure 2. XRD patterns of carbon, PC-impregnated carbon (PC-carbon), and Et_4NBF_4–PC-impregnated carbon (EL-carbon): CDC (a) and ACF (b).

The C1s XPS spectra of both carbons had a broader peak with a shoulder on the higher binding energy side, indicating the presence of surface oxygen groups. The C1s XPS spectra were deconvoluted assuming the following valence states of carbon: C═C at 284.5 eV, C−C at 285.5 eV, C−O at 286.1 eV, C═O at 287.0 eV, and COO− at 289.0 eV (Supporting Information, Figure S2).[21] At the same time, O1s XPS spectra of both carbons were measured. The peak intensity ratios of O1s against C1s were 0.3 for CDC and 0.05 for ACF. The O/C ratios of the graphite crystals of Madagascar graphite, grafoil, and less crystalline graphite are in the range of 0.02−0.07 according to Ohba and Kaneko.[22] The surface oxygen content of CDC is considerably large owing to the very thin pore walls compared with ACF.

Figure 2 shows synchrotron XRD patterns of porous carbons, PC impregnated carbons, and PC electrolytic solution-impregnated carbons at 303 K. ACF has three broad peaks around 16.9, 30, and 52 nm^{-1}, which are assigned to (002), (100) and (101), and (110) reflections of graphite. On the other hand, CDC has almost no peak around 14.9 nm^{-1}, being an obscure shoulder; in-plane reflections are observed around 30 and 52 nm^{-1}, being close to ACF. The XRD feature of CDC suggests the presence of extremely thin graphitic pore walls. Probably CDC has a single curved graphene-like wall structure, agreeing with the N_2 adsorption data and molecular dynamics simulation.[23,24] Also these structural features of CDC are in agreement with the previous studies.[23,24] The XRD patterns of PC-impregnated and PC electrolytic solution impregnated samples of CDC and ACF are similar to each other, and they have three peaks near the *s* values of ACF. However, the peak at the smallest *s* shifts slightly to a smaller value compared with those of the pure carbon, although CDC has a shoulder peak at the low *s* value. The most intense peak positions around s = 14−17 nm^{-1} are summarized in Table 2. The right-side shift of the main peak of bulk PC and PC−Et_4NBF_4 solution is observed by confinement of PC and PC−Et_4NBF_4 solution for both carbons. The peak position of PC and PC + Et_4NBF_4 confined in carbon pores is affected by the (002) reflection of carbon samples, and thereby we must correct the reflection by the carbon samples. Figure 3 shows the XRD patterns of PC and PC + Et_4NBF_4 confined in carbon pores of CDC and ACF after careful correction procedures.[6,14] The XRD patterns of bulk PC and bulk Et_4NBF_4–PC solution are also shown for comparison. The strong peaks around s = 14−15 nm^{-1} of confined PC and Et_4NBF_4–PC solution shift to the right compared with those of bulk PC and the solution. In addition to the strong peak around s = 14−15 nm^{-1}, confined PC and Et_4NBF_4–PC solution have very broad peaks around 31 and 55 nm^{-1}, whereas it is quite difficult to observe the XRD peaks of the bulk PC and Et_4NBF_4–PC solution at the corresponding *s*-regions. Consequently, confined PC and PC + Et_4NBF_4 should have more ordered and closely packed structures than bulk PC liquid. This explanation can be explicitly shown by the electron radial distribution function (ERDF) analysis of these XRD patterns. Figure 4 shows the ERDFs of PC confined in pores of CDC and ACF, in comparison with bulk PC. Confined PC has a similar nearest-neighbor peak at about 0.48 nm, clearly shifted to a shorter distance by 0.05−0.06 nm compared with that of bulk PC. Also, the amplitude of the confined PC is larger than that of bulk PC. Ohba et al. evaluated the PC intermolecular structure in the carbon slit pore with grand canonical Monte Carlo (GCMC) simulation using a 13-centered model for a rigid PC molecule.[25] The simulation predicts both the shorter distance shift of the nearest-neighbor peak and enhancement of the amplitude for the confined PC molecules, as observed

Table 2. Position of the Most Intense Peak (nm^{-1})

PC bulk	EL bulk	CDC	ACF	PC-CDC	EL-CDC	PC-ACF	EL-ACF
13.6	13.5	14.9	16.9	14.5	14.6	15.8	16.1

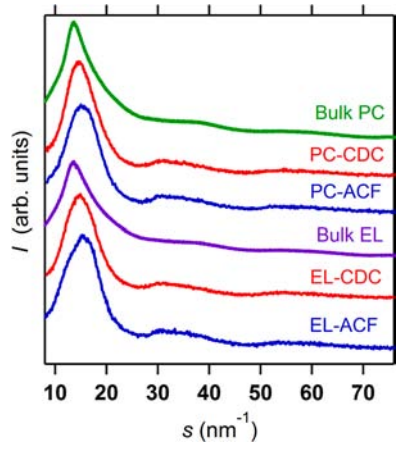

Figure 3. Corrected XRD patterns of PC and Et_4NBF_4–PC confined in pores of CDC and ACF and the XRD pattern of bulk PC at 303 K.

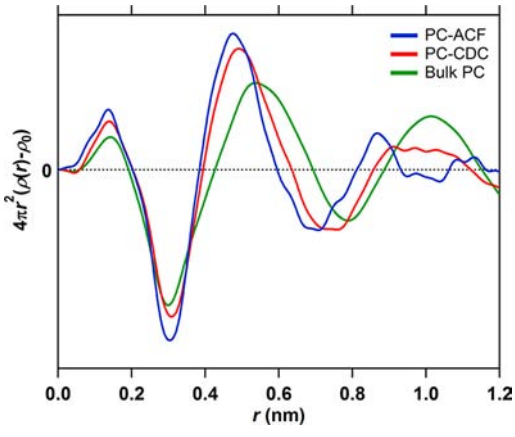

Figure 4. Electron radial distribution functions of PC impregnated in pores of CDC and ACF, in comparison with bulk PC.

above. Therefore, PC molecules in pores are packed in a denser way than in the bulk PC. Also, the effect of confinement of PC molecules in the pores is observed in the long-range structure. The second nearest-neighbor peak (at about 1 nm) of the confined PC is shifted to a shorter distance as well. This shift also indicates a dense packing of PC molecules in the pore space. PC molecules in the pores of ACF have a sharper second peak than those of CDC, while the second peak of PC molecules in pores of CDC is very wide. Consequently, the carbon space of ACF leads to a considerably more ordered packing of solvent molecules than that in CDC; the pore space of CDC should be too narrow to construct the higher packing structure, even though the average pore width difference between ACF and CDC is only 0.03 nm. The fine control of the pore width of ACF is more difficult than CDC, and thereby XRD analysis using a series of CDC samples having different pore widths must be carried out in future. Figure 5 shows the

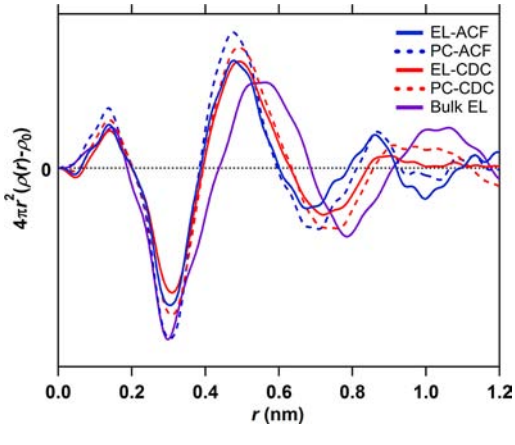

Figure 5. Electron radial distribution functions of PC, electrolyte PC solutions confined in pores, and the bulk electrolyte solution.

ERDFs of Et_4NBF_4–PC and PC confined in the pores and the bulk solution. The addition of Et_4NBF_4 to PC does not change remarkably the ERDF of the bulk PC since the nearest-neighbor peak does not shift. However, a decrease of the amplitude of the nearest-neighbor peak is observed upon addition of the salt in the constrained solution, although such change is not observed in the bulk solution (Figure 2). This could stem from the less ordered packing of bulky Et_4N ions. They can induce a partial disordering in the highly packed PC molecular assembly in the pores. As PC is a polar molecule and the Coulombic interaction affects the intermolecular alignment of PC molecules, the above result can be also interpreted by the partial disordering of the PC molecular assembly through the local electrostatic interaction around ions.

Further insight of intermolecular structures in the absence and presence of Et_4NBF_4 could be obtained by the RMC analysis of XRD patterns, even though the RMC cannot provide a conclusive structure, but a plausible one. Figure 6a

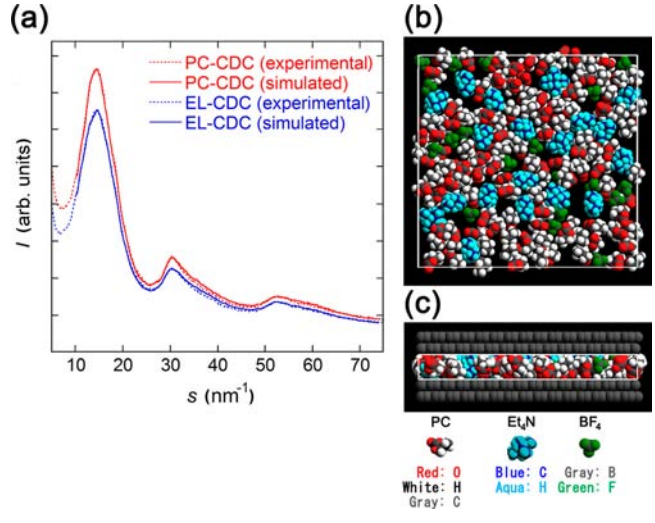

Figure 6. Agreement between the experimental and RMC-simulated XRD patterns (a) for PC and Et_4NBF_4–PC confined in pores of CDC and top (b) and side (c) views of snapshots of Et_4NBF_4–PC solution in the slit pores from RMC simulation.

shows an excellent agreement between the experimental and RMC-simulated XRD patterns of PC and Et_4NBF_4–PC solution confined in pore of CDC. Snapshots of Figure 6, parts b and c, show an irregular structure with isolated Et_4N^+ ions which do not form ion pairs with BF_4^-. At the same time, we can see that PC and Et_4N^+ molecules are vertically oriented against the pore walls, as shown in Figure 6c. In these narrow pores of 0.7 nm width, the long axis of PC and Et_4N^+ fits the slit width of the pore. Therefore, an unusual vertical alignment of PC and Et_4N^+ leads to a denser packing. The molecular alignment in the pore can be better understood from the distribution of PC molecules and the component atoms of the PC molecule in the pore space through the snapshot analysis. Figure 7 shows such distributions for Et_4NBF_4–PC in the pore of CDC and ACF. Here the pore wall is assumed to be a completely smooth basal plane of graphite, and thereby discerning of CDC and ACF is carried out by the different slit widths. Generally speaking, both distributions are very close to each other. Nevertheless we can notice that PC molecules are most distributed near the center in the smaller CDC pore compared with those in the wider ACF pore. The analysis of the atom distribution in the PC molecule can provide information on the orientation of the molecule. The PC molecule has three antisymmetrical oxygen atoms. Accordingly, a higher distribution of oxygen atoms and carbon atoms indicates the orientational direction of the PC molecule. Figure 8 shows two representative molecular orientation models of the PC molecule in the slit pore. One is standing up against the pore wall and another is parallel to the pore wall. Both orientations give completely different atomic distributions

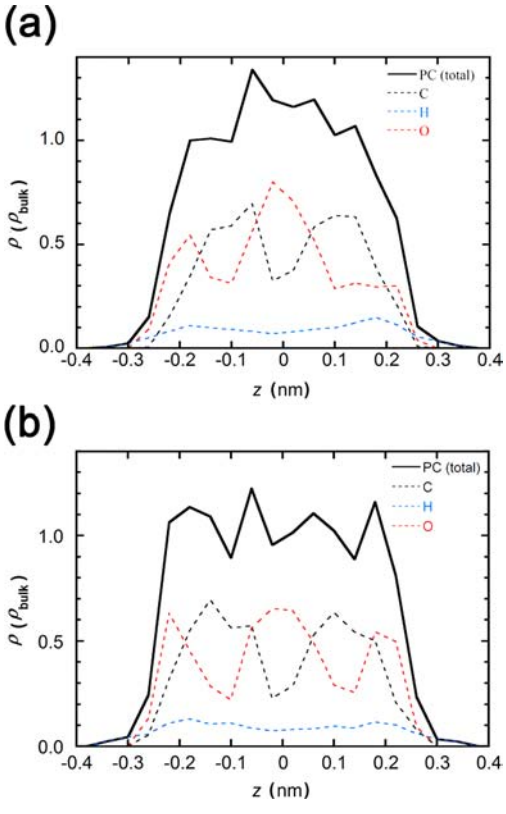

Figure 7. Distribution of PC molecule and the component atoms in the PC molecule along the slit width of CDC (a) and ACF (b).

along the slit width direction. The atomic distribution from the snapshot agrees with the vertical orientation, if we allow two identical orientations in the slit space. Fundamental features of the vertical alignment are similar in the pores of CDC and ACF. PC molecules may be slightly tilted in the narrower pore of CDC, which should lead to the observed disordered second nearest-neighbor structure. The effect of addition of Et_4NBF_4 can be examined using the distribution of molecules as well, although we cannot discuss the orientation of Et_4N^+ ions themselves, because the molecular number is too small for getting the average information. As the molecular shape of Et_4N^+ is very different from that of PC, a partial disorientation of PC molecules occurs, considering the decrease in the amplitude of the nearest-neighbor peak. However, still there are many vertically aligned PC molecules in the pore. Thus, PC molecules should have very unusual intermolecular interactions in the very small carbon pores of about 0.7 nm.

CONCLUSIONS

On the basis of ERDF and RMC analyses, we indicated the vertical alignment of PC molecules interacting with Et_4N^+ and BF_4^- which are confined in extremely narrow slit pores of CDC and ACF. The nearest PC−PC distance is 0.05−0.06 nm shorter than that in the bulk solution, showing dense packing of PC molecules in the pores. It is essentially important that PC molecules can have the most dense assembly structure according to the nanoscale pore geometry. Future efforts should be directed toward unveiling the structure of the PC-based molecular assemblies confined in the subnanoscale pores under the electrical potential.

■ ASSOCIATED CONTENT

Ⓢ Supporting Information

TG analysis of EL-ACF and EL-CDC and XPS spectra of CDC and ACF. This material is available free of charge via the Internet at http://pubs.acs.org.

■ AUTHOR INFORMATION

Corresponding Author

*E-mail: kkaneko@shinshu-u.ac.jp.

Notes

The authors declare no competing financial interest.

■ ACKNOWLEDGMENTS

T.F. and K.K. were supported by Exotic Nanocarbons, Japan Regional Innovation Strategy Program by the Excellence, JST. The synchrotron experiments were performed at the BL02B2 of SPring-8 with the approval of the Japan Synchrotron Radiation Research Institute (JASRI) (proposal nos. 2011B1245, 2010A1601, 2009B1480, and 2009A1417). Y.G. and J.S. were supported by the Partnership University Fund (PUF). P.S. was supported by the Partnership University Fund (PUF) and the European Research Council (Advanced Grant No. ERC-2011-AdG, project no. 291543—IONACES).

■ REFERENCES

(1) Sheng, K.; Sun, Y.; Li, C.; Yuan, W.; Shi, G. Ultrahigh-Rate Supercapacitors Based on Electrochemically Reduced Graphene Oxide for AC Line-Filtering. *Sci. Rep.* **2012**, *2*, 247.

(2) Lang, X.; Hirata, A.; Fujita, T.; Chen, M. Nanoporous Metal/Oxide Hybrid Electrodes for Electrochemical Supercapacitors. *Nat. Nanotechnol.* **2011**, *6*, 232−236.

(3) Mai, L.-Q.; Yang, F.; Zhao, Y.-L.; Xu, X.; Xu, L.; Luo, Y.-Z. Hierarchical $MnMoO_4/CoMoO_4$ Heterostructured Nanowires with Enhanced Supercapacitor Performance. *Nat.Commun.* **2011**, *2*, 381.

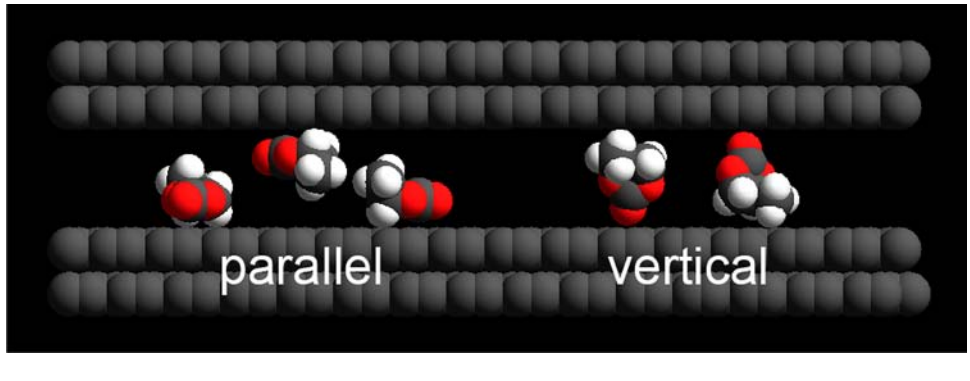

Figure 8. Orientation model of PC molecules in a graphite slit pore.

(4) Xie, X. N.; Lee, K. K.; Wang, J.; Loh, K. P. Polarizable Energy-Storage Membrane Based on Ionic Condensation and Decondensation. *Energy Environ. Sci.* **2011**, *4*, 3960−3965.
(5) Pech, D.; Brunet, M.; Durou, H.; Hueng, P.; Mochalin, V.; Gogotsi, Y.; Taberna, P.-L.; Simon, P. Ultrahigh-Power Micrometre-Sized Supercapacitors Based on Onion-Like Carbon. *Nat. Nanotechnol* **2010**, *5*, 651−654.
(6) Iiyama, T.; Nishikawa, K.; Suzuki, T.; Otowa, T.; Hijiriyama, M.; Nojima, Y.; Kaneko, K. Molecular Assembly Structure of CCl_4 in Graphitic Nanospaces. *J. Phys. Chem. B* **1997**, *101*, 3037−3042.
(7) Iiyama, T.; Nishikawa, K.; Suzuki, T.; Kaneko, K. Study of the Structure of a Water Molecular Assembly in a Hydrophobic Nanospace at Low Temperature with in situ X-Ray Diffraction. *Chem. Phys. Lett.* **1997**, *274*, 152−158.
(8) Urita, K.; et al. Confinement in Carbon Nanospace-Induced Production of KI Nanocrystals of High-Pressure Phase. *J. Am. Chem. Soc.* **2011**, *133*, 10344−10347.
(9) Ohkubo, T.; Konishi, T.; Hattori, Y.; Kanoh, H.; Fujikawa, T.; Kaneko, K. Restricted Hydration Structures of Rb and Br Ions Confined in Slit-Shaped Carbon Nanospace. *J. Am. Chem. Soc.* **2002**, *124*, 11860−11861.
(10) Merlet, C.; Rotenberg, B.; Madden, P. A.; Taberna, P.-L.; Simon, P.; Gogotsi, Y.; Salanne, M. On the Molecular Origin of Supercapacitance in Nanoporous Carbon Electrodes. *Nat. Mater.* **2012**, *11*, 306−310.
(11) Kondrat, S.; Kornyshev, A. A. Superionic State in Double-Layer Capacitors with Nanoporous Electrodes. *J. Phys.: Condens. Matter* **2011**, *23*, 022201.
(12) Kondrat, S.; Pérez, C. R.; Presser, V.; Gogotsi, Y.; Kornyshev, A. A. Effect of Pore Size and Its Dispersity on the Energy Storage in Nanoporous Supercapacitors. *Energy Environ. Sci.* **2012**, *5*, 6474−6479.
(13) Huang, J.; Sumpter, B. G.; Meunier, V. Theoretical Model for Nanoporous Carbon Supercapacitors. *Angew. Chem., Int. Ed.* **2008**, *47*, 520−524.
(14) Tanaka, A.; Iiyama, T.; Ohba, T.; Ozeki, S.; Urita, K.; Fujimori, T.; Kanoh, H.; Kaneko, K. Effect of a Quaternary Ammonium Salt on Propylene Carbonate Structure in Slit-Shape Carbon Nanopores. *J. Am. Chem. Soc.* **2010**, *132*, 2112−2113.
(15) Chmiola, J.; Yushin, G.; Gogotsi, Y.; Portet, C.; Simon, P.; Taberna, P. L. Anomalous Increase in Carbon Capacitance at Pore Sizes Less Than 1 Nanometer. *Science* **2006**, *313*, 1760−1763.
(16) Bandosz, T. J.; Biggs, M.; Gubbins, K. E.; Iiyama, T.; Hattori, Y.; Kaneko, K.; Pikunic, J.; Thomson, K. T. *Chemistry and Physics of Carbon*; Marcel Dekker: New York, 2001; pp 41−228.
(17) Palmer, J. C.; Moore, J. D.; Brennan, J. K.; Gubbins, K. E. Adsorption and Diffusion of Argon in Disordered Nanoporous Carbons. *Adsorption* **2011**, *17*, 189−199.
(18) Nguyen, T. X.; Bhatia, S. K. Some Anomalies in the Self-Diffusion of Water in Disordered Carbons. *J. Phys. Chem. C* **2012**, *116*, 3667−3676.
(19) Setoyama, N.; Suzuki, T.; Kaneko, K. Simulation Study on the Relationship between a High Resolution αs-Plot and the Pore Size Distribution for Activated Carbon. *Carbon* **1998**, *36*, 1459−1467.
(20) Kaneko, K.; Ishii, C.; Ruike, M.; Kuwabara, H. Origin of Superhigh Surface Area and Microcrystalline Graphitic Structures of Activated Carbons. *Carbon* **1992**, *30*, 1075−1088.
(21) Utsumi, S.; Honda, H.; Hattori, Y.; Kanoh, H.; Takahashi, K.; Sakai, H.; Abe, M.; Yudasaka, M.; Iijima, S.; Kaneko, K. Direct Evidence on C-C Single Bonding in Single-Wall Carbon Nanohorn Aggregates. *J. Phys. Chem. C* **2007**, *111*, 5572−5575.
(22) Ohba, T.; Kaneko, K. Surface Oxygen-Dependent Water Cluster Growth in Carbon Nanospaces with GCMC Simulation-Aided in situ SAXS. *J. Phys. Chem. C* **2007**, *111*, 6207−6214.
(23) Palmer, J. C.; Llobet, A.; Yeon, S.-H.; Fischer, J. E.; Shi, Y.; Gogotsi, Y.; Gubbins, K. E. Modeling the Structural Evolution of Carbide-Derived Carbons Using Quenched Molecular Dynamics. *Carbon* **2010**, *48*, 1116−1123.
(24) Laudisio, G.; Dash, R. K.; Singer, J. P.; Yushin, G.; Gogotsi, Y.; Fischer, J. E. Carbide-Derived Carbons: A Comparative Study of Porosity Based on Small-Angle Scattering and Adsorption Isotherms. *Langmuir* **2006**, *22*, 8945−8950.
(25) Ohba, T.; Kaneko, K.; Kanoh, H. Local Ordered Structure of Propylene Carbonate in Slit-Shaped Carbon Nanopores by GCMC Simulation. *ISRN Nanotechnol.* **2011**, *2011*, Article ID 708927, 5 pages.